Carbohydrate Polymers 94 (2013) 63–70

Contents lists available at SciVerse ScienceDirect

Carbohydrate Polymers

journal homepage: www.elsevier.com/locate/carbpol

The composites based on plasticized starch and graphene oxide/reduced graphene oxide

Tiantian Ma [a], Peter R. Chang [b], Pengwu Zheng [c], Xiaofei Ma [a,*]

[a] Chemistry Department, School of Science, Tianjin University, Tianjin 300072, China
[b] Bioproducts and Bioprocesses National Science Program, Agriculture and Agri-Food Canada, 107 Science Place, Saskatoon, SK S7N 0X2, Canada
[c] School of Pharmacy, Jiangxi Science and Technology Normal University, Nanchang, Jiangxi 330013, China

ARTICLE INFO

Article history:
Received 28 September 2012
Received in revised form 4 January 2013
Accepted 6 January 2013
Available online 11 January 2013

Keywords:
Polymer–matrix composites (PMCs)
Thermal analysis
Casting
Graphene oxide

ABSTRACT

The graphite was oxidized to prepare graphene oxide (GO), and GO was reduced by glucose to obtain reduced graphene oxide (RGO) sheet. There were abundant and residual oxygen-containing groups on GO and RGO, respectively. Compared to graphite, the GO and RGO sheets appeared flat and transparent, and the aqueous suspensions followed the Lambert–Beer's law well. The composites were also fabricated by using GO and RGO as the filler in plasticized-starch (PS) matrix. Because of more oxygen-containing groups, GO could form the stronger interaction with PS matrix than RGO. And GO/PS composites exhibited better tensile strength, elongation at break and moisture barrier than RGO/PS composites, but lower thermal stability. GO/PS composites could protect against UV light, while the conductivities of RGO/PS composites could reach 1.07×10^{-4}, 6.92×10^{-4} and 0.01 S/cm, respectively stored at RH50, 75 and 100%.

1. Introduction

Nanocomposites based on natural polymers and nanometer-scale fillers are of scientific and industrial interest for use as alternatives to traditional plastic materials such as polyolefins. Due to excessive consumption and poor degradation of plastics, a massive accumulation of plastic waste has been disposed in the environment (Rodríguez, Galotto, Guarda, & Bruna, 2012). As a natural polysaccharide from a great variety of crops, starch has been investigated widely for the potential manufacture of degradable products, including water-soluble pouches for detergents and insecticides, flushable liners and bags, and medical delivery systems and devices (Fishman, Coffin, Konstance, & Onwulata, 2000). The nanometer-scale fillers are often introduced into a plasticized-starch (PS) matrix to improve the tensile strength and water barrier properties, and to add to the functional properties (Sreekumar, Gopalakrishnan, Leblanc, & Saiter, 2010). Recently, carbon materials have also been used as filler in the preparation of PS-based composites. Carbon nanotube (CNT) has been incorporated into PS matrix resulting in enhanced mechanical strength and electrical conductivity (Famá, Pettarin, Goyanes, & Bernal, 2011; Liu, Chang, et al., 2011; Liu, Zhao, Chen, & Yu, 2011; Ma, Yu, & Wang, 2008). Carbon black was also added into PS matrix to obtain electrically conductive composites, prepared by both melt extrusion and microwave radiation (Ma, Chang, Yu, & Lu, 2008). The composites prepared using microwave radiation exhibited better properties, including reinforcing effect, conductivity and water vapor barrier, than those from melt extrusion.

Graphene is a two-dimensional sheet of sp^2-hybridized carbon arranged in a hexagonal lattice with a high surface area, excellent mechanical properties, and electrical conductivity. Recently, much work has focused on mechanically or electrically enhanced polymers using nanosheets of graphene oxide (GO) or reduced graphene oxide (RGO) as nanofillers (Feng, Zhang, Shen, Yoshino, & Feng, 2012; Potts, Dreyer, Bielawski, & Ruoff, 2011). It is well known that good interaction between the filler and matrix is necessary to obtain the best characteristics in composites. The hydrophilic GO can form strong hydrogen bonding interactions with multiple hydroxyl groups in starch due to the various oxygen functional groups of GO, including hydroxyls, epoxides, carbonyls and carboxyls (Li, Liu, & Ma, 2011). After the reduction process, the carbon arranged in the hexagonal lattice was mostly removed, and the RGO exhibited conductivity. The residual oxygen-containing groups on RGO can still form interactions with starch as well. In this study, graphite was oxidized to prepare GO using a modified Hummer's method and reduced by glucose to obtain RGO sheets. The GO and RGO sheets were explored for use as fillers in the preparation of GO/PS and RGO/PS composites with improved mechanical

* Corresponding author. Tel.: +86 22 27406144; fax: +86 22 27403475.
E-mail address: maxiaofei@tju.edu.cn (X. Ma).

0144-8617/$ – see front matter.
http://dx.doi.org/10.1016/j.carbpol.2013.01.007

and moisture barrier properties of the PS matrix, and may find their niche in applications such as ultraviolet–visible absorbance or electrical conductivity.

2. Experimental

2.1. Materials

Potato starch was supplied by Manitoba Starch Products (Manitoba, Canada). Natural graphite flakes were provided by Qingdao Tianhe Graphite Co., Ltd., China. The reagents (37.5% HCl, 98% H_2SO_4, 30% H_2O_2, 30% NH_3) and the analytical grade reagents ($NaNO_3$, $KMnO_4$, glucose, glycerol) were purchased from Tianjin Jiangtian Chemical Reagent Co., Ltd., China.

2.2. Preparation of GO and RGO

The GO was prepared by oxidizing graphite using a modified Hummer's method (Hummers & Offeman, 1958). Concentrated H_2SO_4 (46 mL) and $NaNO_3$ (1 g) were added into a flask and cooled to below 5 °C, followed by the addition of graphite (2 g). Solid $KMnO_4$ (6 g) was gradually added under stirring and stirred for 1 h at below 20 °C. The temperature was then increased and kept at 35 °C for 2 h. 92 mL distilled water was then added, and the temperature was increased to 98 °C for another 15 min. Excess distilled water (150 mL) was added to the mixture followed by 30% H_2O_2 (5 mL). The mixture was immediately centrifuged and the resulting GO sheets were washed three times with 5% aqueous HCl to remove metal ions, and then washed with distilled water to remove the acid. The GO sheets were air dried and dispersed in water.

The GO was reduced by glucose to obtain RGO sheets using the modified method of Wang et al. (2011). Typically, 2 g glucose was added into 250 mL of homogeneous GO dispersion (0.5 mg/mL), followed by stirring for 30 min. Then, 1 mL ammonia solution (30%, w/w) was added and stirred for 10 min. The RGO reaction was then kept at 95 °C for 60 min. The resulting black dispersion was filtered and washed with water several times.

2.3. Preparation of GO/PS and RGO/PS composites

GO and RGO were, respectively, dispersed into solutions of distilled water (100 mL) using ultrasonication for 10 min. The GO loading levels (0, 0.5, 1, 2, 3 and 4 wt%) and RGO loading levels (0, 2, 4, 6 and 8 wt%) were based on starch. Glycerol (1.5 g) and starch (5 g) were added to the obtained GO or RGO suspensions. The mixture was then heated at 90 °C for 0.5 h with constant stirring to plasticize the starch. The mixture was cast into a film and dried in an air-circulating oven at 50 °C. The GO/PS and RGO/PS composite films were preconditioned in a climate chamber at 25 °C and 50% RH for at least 48 h prior to testing.

2.4. Fourier transform infrared spectroscopy (FTIR)

FTIR analysis of graphite, GO, and RGO was performed on a BIO-RAD FTS3000 IR Spectrum Scanner. The sample powders were evenly dispersed in KBr and pressed into transparent sheets for testing.

2.5. Thermogravimetric (TG) analysis

Thermal properties of raw graphite, GO, RGO and the composites were measured with a ZTY-ZP type thermal analyzer. The sample weights were about 15 mg and they were heated from room temperature to 500 °C at a heating rate of 15 °C/min in a nitrogen atmosphere.

2.6. Scanning electron microscopy (SEM)

The graphite and the fracture surfaces of GO/PS composites were viewed by a NanoSEM 430 scanning electron microscope, while GO, RGO, and the fracture surfaces of RGO/PS composites were tested using an S-4800 scanning electron microscope. The graphite, GO, and RGO were, respectively, dispersed into water using ultrasonication for 5 min. The suspension drops were drawn on a glass flake, dried to remove water, and then vacuum coated with gold for SEM testing. The GO/PS and RGO/PS composites were cooled in liquid nitrogen and then broken. The fracture faces were vacuum coated with gold for SEM testing.

2.7. UV–visible (UV–vis) spectra

The UV–visible spectra of the aqueous solutions with different concentrations of graphite, GO, and RGO and the GO/PS composites were recorded from 200 to 800 nm using a UV–vis spectrophotometer model U-1800, Hitachi Company. The UV–visible spectrums of GO/PS composites were recorded using a blank glass plate as reference.

2.8. Dispersion in aqueous solutions

The graphite, GO, and RGO were, respectively, added to H_2O and the mixtures were dispersed by ultrasonication for 10 min. And water was added to obtain the solution with low concentration. Photos of the graphite, GO, and RGO dispersions were taken with a digital camera.

2.9. Mechanical testing

The Testometric AX M350-10KN Materials Testing Machine was operated at a crosshead speed of 50 mm/min for tensile testing (ISO 1184-1983 standard). The data was averaged over 6–8 specimens.

2.10. Water vapor permeability (WVP)

WVP tests were carried out by ASTM method E96 (1996) with some modifications (Guilherme, Mattoso, Gontard, Guilbert, & Gastaldi, 2010). The films were cut into circles, sealed over with melted paraffin, and stored in a desiccator at 25 °C. RH (relative humidity) 0% was maintained using anhydrous calcium chloride in the cell. Each cell was placed in a desiccator containing saturated sodium chloride to provide a constant RH 75%. Water vapor transport was determined by the weight gain of the permeation cell. Changes in the weight of the cell were recorded as a function of time. Slopes were calculated by linear regression (weight change vs. time) and correlation coefficients for all reported data were >0.99. The water vapor transmission rate (WVTR) was defined as the slope (g/s) divided by the transfer area (m^2). After the permeation tests, film thickness was measured and WVP ($g\,Pa^{-1}\,s^{-1}\,m^{-1}$) was calculated as

$$WVP = \frac{WVTR}{P(R_1 - R_2)} \cdot x \quad (1)$$

where P is the saturation vapor pressure of water (Pa) at the test temperature (25 °C); R_1 is the RH in the desiccator; R_2, the RH in the permeation cell; and x is the film thickness (m). Under these conditions, the driving force $[P(R_1 - R_2)]$ is 1753.55 Pa.

2.11. Electrical conductivity

The RGO/PS composite films were stored in closed chambers over various materials at 20 °C for several days. The materials used were substantive 35.64% $CaCl_2$ solution, saturated NaCl solution,

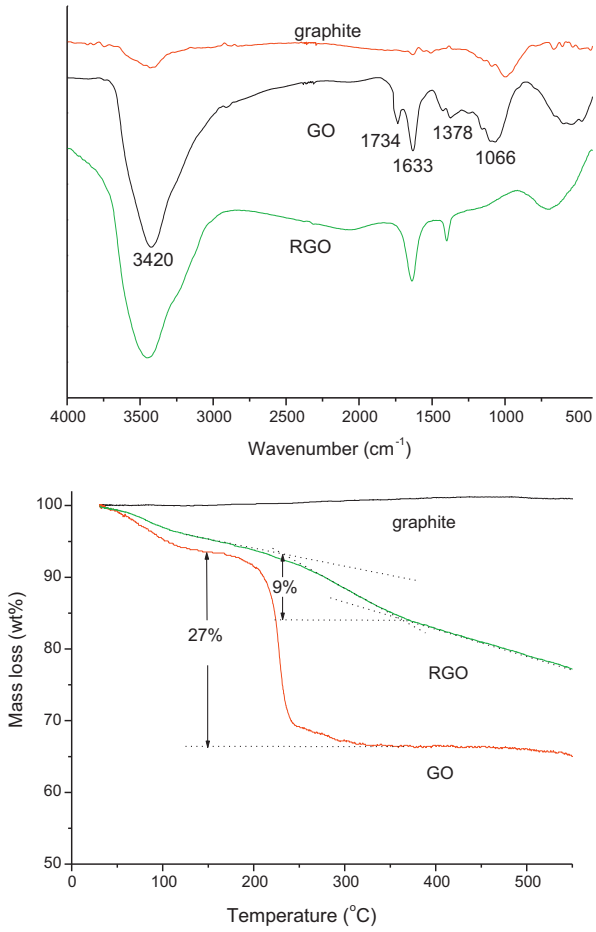

Fig. 1. FTIR spectra (a) and TG (b) of raw graphite, GO and RGO.

and distilled water which provided RH's of about 50, 75 and 100%, respectively. Volume resistivity measurements were performed on the composite films. The films with dimensions of 30 mm × 5 mm and 0.5 mm thickness were measured using a Model ZL7 electrometer (SPSIC Huguang Instruments & Power Supply Branch, China) using a four-point test fixture.

3. Results and discussion

3.1. Characterization of GO and RGO

In Fig. 1(a), the FTIR spectrum of GO shows a broad band at 3420 cm^{-1}, related to the vibration and deformation bands of —OH and —COOH. The absorption bands at 1633 and 1734 cm^{-1} were ascribed to aromatic C=C and carboxyl groups. Other C—O groups such as C—OH (1378 cm^{-1}) and C—O (1066 cm^{-1}) were also clearly observed (Li et al., 2011). These main characteristic peaks were similar to the GO from the literature (Wang et al., 2009). These demonstrated that the GO had an abundance of oxygen containing groups (Zhou et al., 2011). As shown in RGO of Fig. 1(a), the significant reduction of the intensity of all oxygen containing groups suggested the efficient conversion of GO to RGO.

TG has been used to estimate the oxidation degree of GO and RGO (Wojtoniszak, Chen, & Kalenczuk, 2012). TG plots of raw graphite, GO and RGO were shown in Fig. 1(b). There was a mass loss for GO and RGO below 100 °C attributed to the removal of adsorbed water (Paredes, Villar-Rodil, Martinez-Alonso, & Tascon, 2008). The mass loss at about 200 °C was corresponded to the removal of oxygen-containing functional groups (Wojtoniszak et al., 2012).

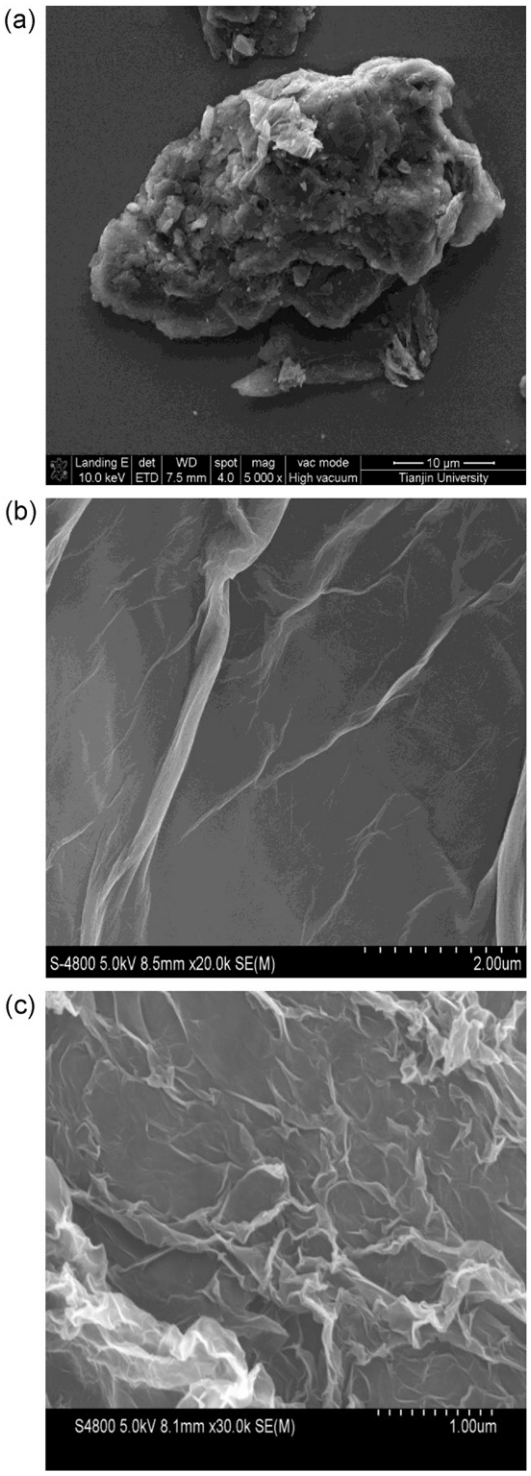

Fig. 2. SEM of raw graphite (a), GO (b), and RGO (c).

The TG analysis indicated that the oxygen containing groups in GO was about 27 wt%, and about 7 wt% of oxygen containing groups did not undergo reduction in RGO.

Raw graphite (Fig. 2a) consisted of randomly aggregated, thin, crumpled sheets closely associated with each other. Compared with graphite, the GO sheets (Fig. 2b) appeared flat and transparent, with some wrinkles and folding on the surface. The RGO image (Fig. 2c) clearly revealed the ultrathin and homogeneous graphene sheets. Such sheets were at times folded or continuous and it was possible

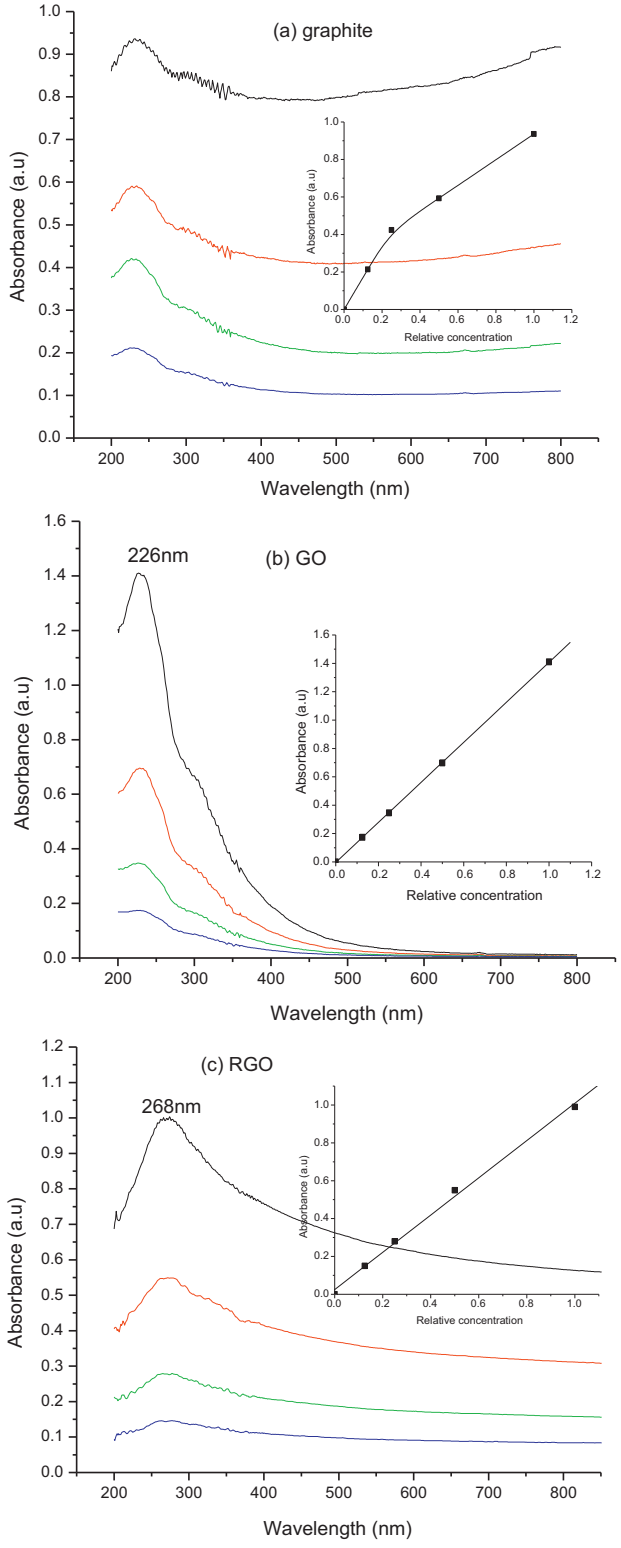

Fig. 3. UV–visible spectra of raw graphite (a), GO (b) and RGO (c) in water with increasing concentration from bottom to top. The insets are Lambert–Beer's plots for the absorption peaks of GO at 226 nm and RGO at 268 nm.

to distinguish the edges of individual sheets, including kinked and wrinkled areas (Tang et al., 2009).

Fig. 3 exhibits the UV–vis spectra of graphite, GO, and RGO with different concentrations in distilled water. Fig. 3(a) shows a non-linear relationship between the observed absorption peak and the graphite concentrations indicating that graphite was not stable in water. The UV–vis spectra of GO exhibited an obvious characteristic feature that can be used as an identification tool: maximum absorption peak at about 226 nm, as shown in Fig. 3(b), corresponding to π–π^* transition of aromatic C—C bonds (Luo, Zhang, Liu, & Sun, 2011). The linear relationship between the observed absorption peak and the GO concentrations indicated that aggregation (or precipitation) of GO sheets did not occur in the tested concentration range (Wu et al., 2007). GO exhibited good stability in water because of the hydrophilic oxygen containing groups and the thin layers of each GO sheet. When GO was reduced to RGO, the position of the absorption peak red shifted to 268 nm (Fig. 3c). And RGO exhibited lower absorbance. This phenomenon has also been previously reported and used as a monitoring tool for the reduction of GO (Luo et al., 2011). The basically linear relationship indicated that RGO also had good stability in water, which was related to the residual oxygen containing groups and the thin layers of each RGO sheet.

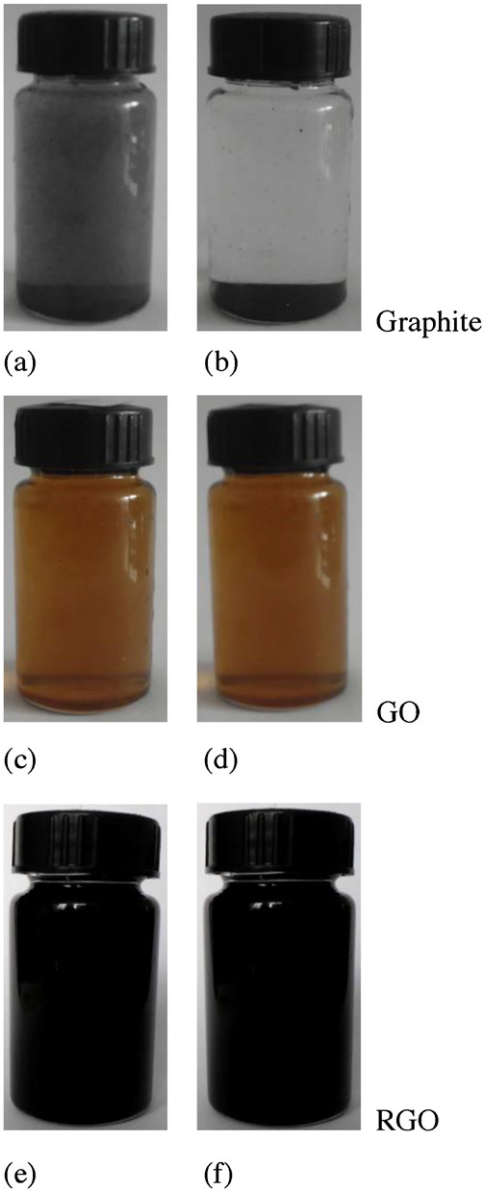

Fig. 4. Photographs of dispersions of graphite (a and b), GO (c and d), and RGO (e and f) in water after 0 h (a, c and e), 10 min (b), and one month (d and f).

As shown in Fig. 4(a) and (b), the graphite suspension in water is not stable, and within several minutes a graphite precipitate was

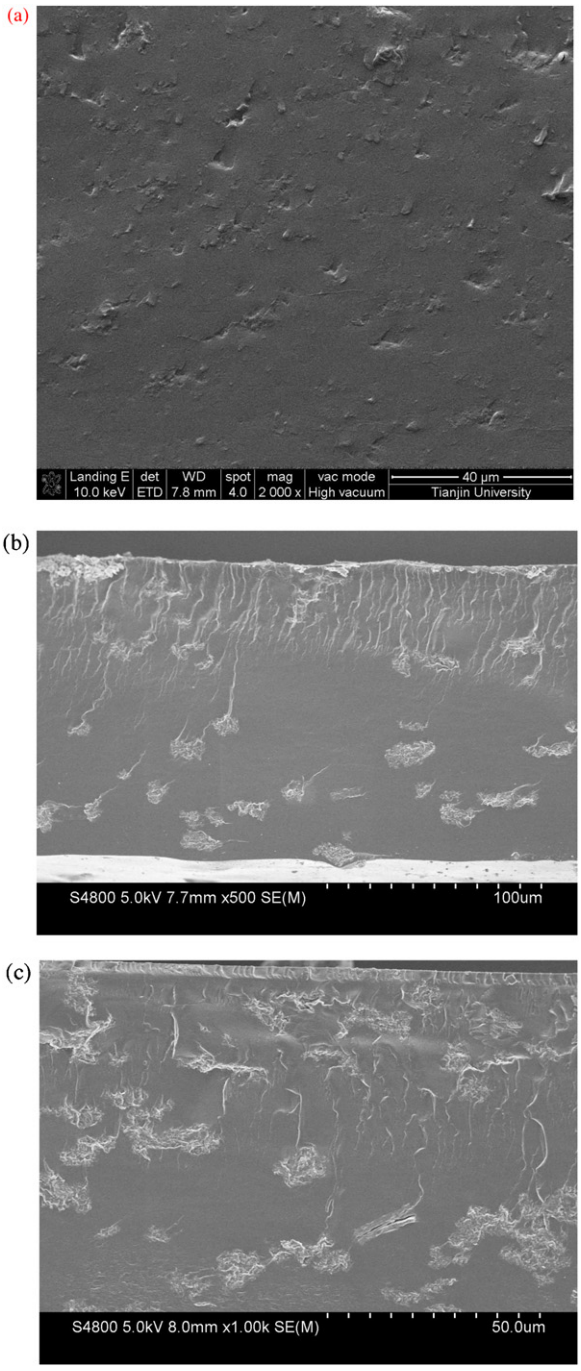

Fig. 5. SEM micrographs of the fragile fractured surfaces of composites with loading levels of 3 wt% GO (a), 3 wt% RGO (b) and 6 wt% RGO (c).

observed. However, the golden GO (Fig. 4c and d) and the dark RGO (Fig. 4e and f) readily dispersed in water with mild ultrasonic treatment, and the formed suspension was stable for one month. The good stability of GO and RGO suspension in water was very important for the preparation of starch-based composites using the casting process.

3.2. Morphology of the composites

The SEM images of the fracture surfaces of the GO/PS and RGO/PS composites are shown in Fig. 5. GO sheets were found to be uniformly dispersed in the PS matrix in Fig. 5(a). It was similar to the earlier report (Xu, Hong, Bai, Li, & Shi, 2009). In Fig. 5(b) and

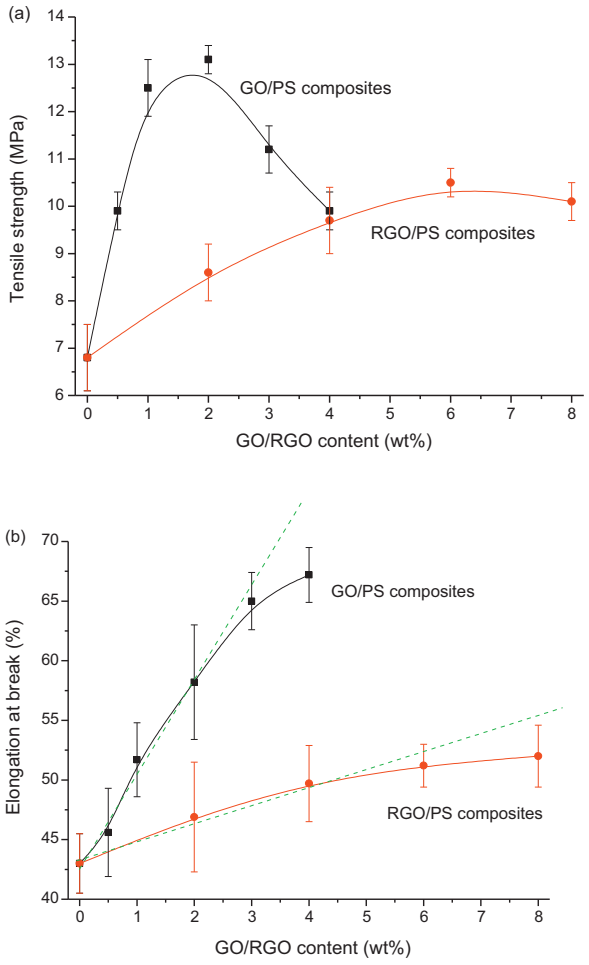

Fig. 6. Effect of GO/RGO content on tensile strength (a) and elongation at break (b) of the composites.

(c), the surfaces and the edges of the RGO sheets were clearly observed in a PS matrix with 3 and 6 wt% RGO loaded. RGO sheets were well dispersed in the PS matrix, but they looked more like a lump with an irregular shape than a flat sheet and exhibited a rough surface and rounded edges. This may have been caused by the evaporation of water upon drying/heating during the casting process (Mahmoud, 2011). In addition, GO appeared to be covered by the PS matrix, which was related to stronger interfacial interactions between GO and the matrix. GO sheets with more oxygen-containing groups of could form better hydrogen bond interactions with starch than RGO sheets.

3.3. Mechanical properties of the composites

Fig. 6 reveals the effect of GO and RGO content on the mechanical properties of the nanocomposites. As shown in Fig. 6(a), both GO and RGO had an obvious reinforcing effect on the PS matrix. The tensile strength of PS was only 6.8 MPa. For GO/PS composites, the tensile strength reached a maximum of 13.1 MPa at a loading level of 2 wt% GO, while the tensile strength of RGO/PS composites exhibited a maximum of 10.5 MPa at a higher loading level of 6 wt% RGO. The improvement in tensile strength was related to good interfacial interaction, which may have lead to a higher efficiency of stress transfer from the PS matrix to the GO/RGO fillers (Franco-Marquès et al., 2011). GO filler formed stronger interactions with the PS matrix than RGO filler because GO had abundant oxygen containing groups which formed hydrogen-bonding interactions with

the starch hydroxyl groups. It was observed that the tensile strength decreased when the loading was more than 2 wt% for GO/PS composites and for 6 wt% for RGO/PS composites. The agglomeration of GO/RGO could reduce the effective cross-linking points and the interaction between GO/RGO and PS matrix. The agglomeration of GO with abundant oxygen containing groups could take place at the lower loading than that of RGO.

Fig. 6(b) shows that the elongation at break of the composites exhibited the same tendency as tensile strength when GO and RGO fillers were added into the PS matrix. The elongation at break of the GO/PS composites increased by about 25% when the GO loading level increased from 0 to 4 wt%, while that of the RGO/PS composites was enhanced by only 10% with increasing RGO loading from 0 to 8 wt%. The incorporation of GO sheets simultaneously improved the strength and elongation at break of PS films, which was extraordinary as compared with many RGO/polymer composites (Kim, Abdala, & Macosko, 2010). It could be related to the sheet structure of GO/RGO filler, which could form the good interaction with PS matrix, and at the same time make starch molecules slightly slip at the surface of GO/RGO sheets in the tensile testing. Similarly, GO addition improved the tensile strength and elongation at break of chitosan films (Pan, Wu, Bao, & Li, 2011). The agglomeration of GO/RGO fillers could influence the elongation at break. As illustrated by dash lines in Fig. 6(b), the increasing of elongation at break slowed with the increasing of GO/RGO filler contents, when the filler loading was higher than 2–3 wt% for GO/PS composites and 4–6 wt% for RGO/PS composites.

3.4. Thermal stability of the composites

TG and DTG curves of GO/PS and RGO/PS composites are shown in Fig. 7(a). The mass loss of PS before the onset temperature was related to the volatilization of both water and glycerol plasticizer. As revealed by the DTG curves, the degradation of GPS took place at about 314 °C, i.e., the temperature at maximum rate of mass loss. Usually, the better the interaction between the filler and the matrix was, the higher the thermal stability of the composites was. However, GO/PS composites containing 2 wt% GO thermally degraded at 297 °C indicating that the addition of GO unexpectedly decreased the thermal stability of the composites. The decomposition of oxygen functional groups (about 27 wt%) in GO takes place at around 200 °C (as shown in Fig. 1b), which could weaken the interaction between GO filler and PS matrix and simultaneously accelerate the decomposition of starch matrix. In agreement with this result, the addition of GOs also decreased the thermal stability of epoxy resins (Qiu et al., 2011). RGO/PS composites containing 2 wt% RGO degraded at 314 °C. Because the oxygen containing groups (about 9 wt%) in RGO decreased dramatically, RGO/PS composites exhibited better thermal stability than GO/PS composites.

3.5. WVP of composites

Fig. 7(b) exhibits the moisture transport through the composite films with different GO and RGO contents at RH 75%. WVP of GO/PS and RGO/PS composites decreased with increasing filler content. Water vapor easily permeated the PS film and had the highest WVP value of 5.68×10^{-10} g m^{-1} s^{-1} Pa^{-1}. Increasing the GO content from 0 to 4 wt% led to an obvious decrease in the WVP values of GO/PS composites (to 3.2×10^{-10} g m^{-1} s^{-1} Pa^{-1}), while the WVP values for RGO/PS composites only decreased to 3.7×10^{-10} g m^{-1} s^{-1} Pa^{-1} with the higher RGO loading of 8 wt%. Because of the good dispersion of GO and RGO fillers in the PS matrix, GO and RGO sheets probably introduced tortuous paths for water molecules to pass through (Liu, Chang, et al., 2011; Liu, Zhao, et al., 2011). Since GO formed better interactions with the PS matrix than RGO, there were fewer paths for water molecules

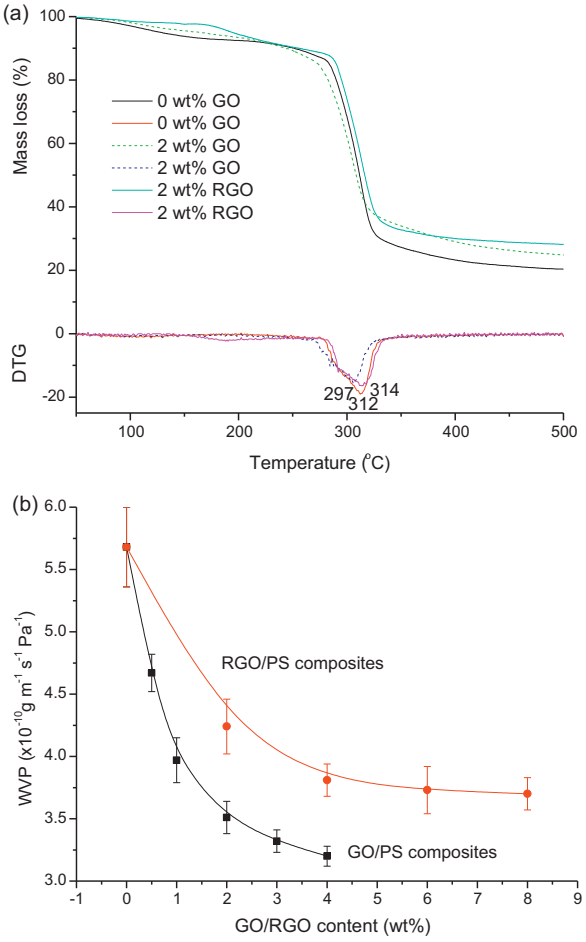

Fig. 7. (a) TG and DTG curves of composites containing 2 wt% GO and 2 wt% RGO. (b) Effect of GO/RGO content on water vapor permeability of the composites.

to pass through in GO/PS composites. Generally, the composites exhibited moisture barrier properties comparable to pure PS film. GO/PS composites with lower GO loading levels had better moisture barrier properties than RGO/PS composites with higher RGO loading.

3.6. UV–vis spectra of GO/PS composites

Fig. 8(a) shows the ultraviolet–visible absorbance of GO/PS composites with different GO contents. The absorbance was remarkably enhanced by the addition of GO sheets compared to the absorbance of pure PS. In the near ultraviolet range (200–400 nm) there was very low absorbance in the pure PS. With increasing GO content, the UV absorbance and the intensity of the peaks increased. The absorbance value peaked at 2.613 for the composite with 2 wt% GO, meaning that the transmittance of UV light was only 0.24%, and most of the UV light was shielded. GO/PS composites could effectively protect against UV light and potentially be applied to UV-shielding materials (Ma, Chang, Yang, & Yu, 2009). RGO/PS composites, however, had no obvious UV absorbance.

3.7. Electrical conductivity of RGO/PS composites

The conductivity of RGO/PS composite films with different RGO contents is shown in Fig. 8(b). After reduction using glucose, the sp^2 hybridized structure of graphites was partly restored, and the conductivity of the composite films was enhanced by the increasing RGO content. By increasing the RGO content from 0 to 2 wt%,

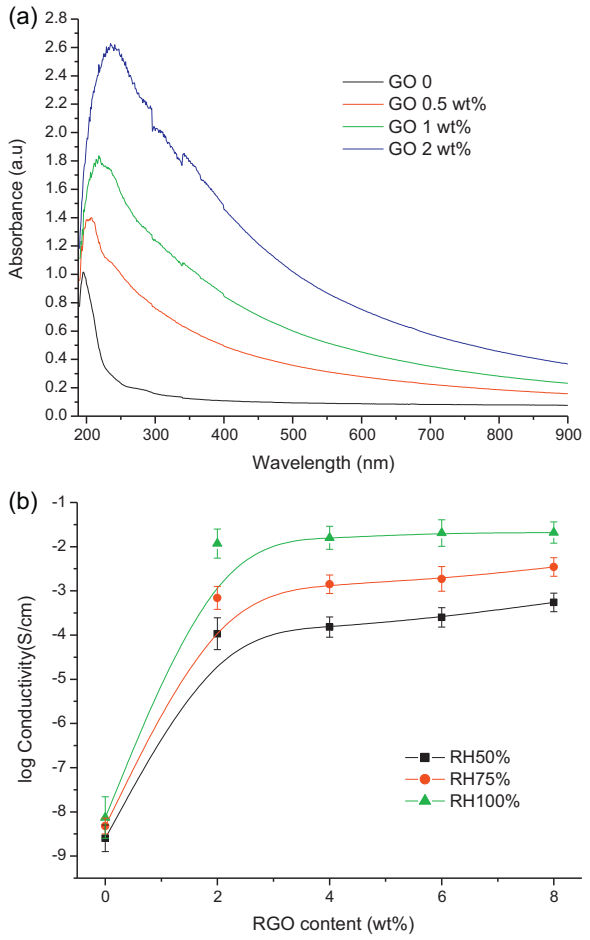

Fig. 8. (a) Ultraviolet–visible absorbance of GO/PS composites. The GO contents are 0, 0.5, 1 and 2 wt% from the bottom curve to the top, respectively. (b) Electrical conductivity of RGO/PS composites with different RGO contents at RH50, 75 and 100%.

the conductivity of the composite films increased by 5–6 orders of magnitude in contrast with PS. The uniformly dispersed RGO improved the conductivity of the PS matrix, probably due to the formation of conductive networks throughout the insulating matrix (Feng et al., 2012). With higher RGO content (>2 wt%), enhancement of the conductivity was not obvious.

The conductivity of RGO/PS composite was dependent on water content. The moisture contents at equilibrium of the composites were about 20%, 30% and 60% at RH 50, 75 and 100%, and the conductivities of RGO/PS composite reached 1.07×10^{-4}, 6.92×10^{-4} and 0.01 S/cm with 2 wt% RGO loading, respectively. The phenomenon could be related to the ion conductance. The RGO/PS composite could be a promising candidate for biosensor and tissue engineering applications. GO/PS composites had poor conductivity because the sp^2 structure in GO was destroyed.

4. Conclusions

GO/PS and RGO/PS composites were prepared using a casting process because both GO and RGO suspensions were stable in water. This stability was ascribed to the hydrophilic oxygen containing groups and the thin layers. The abundant oxygen-containing groups of GO and the residual oxygen-containing groups of RGO could form hydrogen bond interactions with starch. These interactions and the unidirectional, uniform dispersion of GO/RGO sheets in the PS matrix played important roles in improvements to mechanical and moisture barrier properties. RGO/PS composites exhibited better thermal stability than GO/PS composites. GO and RGO added functional properties to the PS matrix such as UV absorbance for GO/PS composites and electrical conductivity for RGO/PS composites. The GO/PS and RGO/PS composites with desirable mechanical properties are some of the most promising candidates for advanced UV shielding, biochemical, or electrochemical materials. In addition, GO and RGO sheets could also be used as fillers for other natural polysaccharide (guar gum, agar, alginate and chitosan) matrixes.

Acknowledgments

The authors acknowledge funding contribution provided by the Innovation Foundation of Tianjin University and the National Natural Science Foundation of China No. 51162011.

References

Famá, L. M., Pettarin, V., Goyanes, S. N., & Bernal, C. R. (2011). Starch/multi-walled carbon nanotubes composites with improved mechanical properties. *Carbohydrate Polymers*, *83*, 1226–1231.
Feng, Y. Y., Zhang, X. Q., Shen, Y. T., Yoshino, K., & Feng, W. (2012). A mechanically strong flexible and conductive film based on bacterial cellulose/graphene nanocomposite. *Carbohydrate Polymers*, *87*, 644–649.
Fishman, M. L., Coffin, D. R., Konstance, R. P., & Onwulata, C. I. (2000). Extrusion of pectin/starch blends plasticized with glycerol. *Carbohydrate Polymers*, *41*, 317–325.
Franco-Marquès, E., Méndez, J. A., Pèlach, M. A., Vilaseca, F., Bayer, J., & Mutjé, P. (2011). Influence of coupling agents in the preparation of polypropylene composites reinforced with recycled fibers. *Chemical Engineering Journal*, *166*, 1170–1178.
Guilherme, M. R., Mattoso, L. H. C., Gontard, N., Guilbert, S., & Gastaldi, E. (2010). Synthesis of nanocomposite films from wheat gluten matrix and MMT intercalated with different quaternary ammonium salts by way of hydroalcoholic solvent casting. *Composites Part A Applied Science and Manufacturing*, *41*, 375–382.
Hummers, W. S., & Offeman, R. E. (1958). Preparation of graphitic oxide. *Journal of the American Chemical Society*, *80*, 1339.
Kim, H., Abdala, A. A., & Macosko, C. W. (2010). Graphene/polymer nanocomposites. *Macromolecules*, *43*, 6515–6530.
Li, R., Liu, C. H., & Ma, J. (2011). Studies on the properties of graphene oxide-reinforced starch biocomposites. *Carbohydrate Polymers*, *84*, 631–637.
Liu, D., Chang, P. R., Deng, S., Wang, C. Y., Zhang, B. J., Tian, Y., et al. (2011). Fabrication and characterization of zirconium hydroxide- carboxymethyl cellulose sodium/plasticized *Trichosanthes Kirilowii* starch nanocomposites. *Carbohydrate Polymers*, *86*, 1699–1704.
Liu, Z. J., Zhao, L., Chen, M. N., & Yu, J. G. (2011). Effect of carboxylate multi-walled carbon nanotubes on the performance of thermoplastic starch nanocomposites. *Carbohydrate Polymers*, *83*, 447–451.
Luo, D. C., Zhang, G. X., Liu, J. F., & Sun, X. M. (2011). Evaluation criteria for reduced graphene oxide. *The Journal of Physical Chemistry C*, *115*, 11327–11335.
Ma, X. F., Chang, P. R., Yu, J. G., & Lu, P. L. (2008). Characterizations of glycerol plasticized-starch (GPS)/carbon black (CB) membranes prepared by melt extrusion and microwave radiation. *Carbohydrate Polymers*, *74*, 895–900.
Ma, X. F., Chang, P. R., Yang, J. W., & Yu, J. G. (2009). Preparation and properties of glycerol plasticized-pea starch/zinc oxide-starch bionanocomposites. *Carbohydrate Polymers*, *75*, 472–478.
Ma, X. F., Yu, J. G., & Wang, N. (2008). Glycerol plasticized-starch/multiwall carbon nanotube composites for electroactive polymers. *Composites Science and Technology*, *68*, 268–273.
Mahmoud, W. E. (2011). Morphology and physical properties of poly(ethylene oxide) loaded graphene nanocomposites prepared by two different techniques. *European Polymer Journal*, *47*, 1534–1540.
Pan, Y. Z., Wu, T. F., Bao, H. Q., & Li, L. (2011). Green fabrication of chitosan films reinforced with parallel aligned graphene oxide. *Carbohydrate Polymers*, *83*, 1908–1915.
Paredes, J. I., Villar-Rodil, S., Martinez-Alonso, A., & Tascon, J. M. D. (2008). Graphene oxide dispersions in organic solvents. *Langmuir*, *24*, 10560–10564.
Potts, J. R., Dreyer, D. R., Bielawski, C. W., & Ruoff, R. S. (2011). Graphene-based polymer nanocomposites. *Polymer*, *52*, 5–25.
Qiu, S. L., Wang, C. S., Wang, Y. T., Liu, C. G., Chen, X. Y., Xie, H. F., et al. (2011). Effects of graphene oxides on the cure behaviors of a tetrafunctional epoxy resin. *Express Polymer Letters*, *5*, 809–818.
Rodríguez, F. J., Galotto, M. J., Guarda, A., & Bruna, J. E. (2012). Modification of cellulose acetate films using nanofillers based on organoclays. *Journal of Food Engineering*, *110*, 262–268.
Sreekumar, P. A., Gopalakrishnan, P., Leblanc, N., & Saiter, J. M. (2010). Effect of glycerol and short sisal fibers on the viscoelastic behavior of wheat flour based thermoplastic. *Composites Part A Applied Science and Manufacturing*, *41*, 991–996.

Tang, L. H., Wang, Y., Li, Y. M., Feng, H. B., Lu, J., & Li, J. H. (2009). Preparation, structure, and electrochemical properties of reduced graphene sheet films. *Advanced Functional Materials*, *19*, 2782–2789.

Wang, J., Gao, Z., Li, Z. S., Wang, B., Yan, Y. X., Liu, Q., et al. (2011). Green synthesis of graphene nanosheets/ZnO composites and electrochemical properties. *Journal of Solid State Chemistry*, *184*, 1421–1427.

Wang, G. X., Wang, B., Park, J. S., Yang, J., Shen, X. P., & Yao, J. (2009). Synthesis of enhanced hydrophilic and hydrophobic graphene oxide nanosheets by a solvothermal method. *Carbon*, *47*, 68–72.

Wojtoniszak, M., Chen, X. C., & Kalenczuk, R. J. (2012). Synthesis, dispersion and cytocompatibility of graphene oxide and reduced graphene oxide. *Colloids and Surfaces B: Biointerfaces*, *89*, 79–85.

Wu, Z. G., Feng, W., Feng, Y. Y., Liu, Q., Xu, X. H., Sekino, T., et al. (2007). Preparation and characterization of chitosan-grafted multiwalled carbon nanotubes and their electrochemical properties. *Carbon*, *45*, 1212–1218.

Xu, Y. X., Hong, W. J., Bai, H., Li, C., & Shi, G. Q. (2009). Strong and ductile poly(vinyl alcohol)/graphene oxide composite films with a layered structure. *Carbon*, *47*, 3538–3543.

Zhou, X. J., Zhang, J. L., Wu, H. X., Yang, H. J., Zhang, J. Y., & Guo, S. W. (2011). Reducing graphene oxide via hydroxylamine: A simple and efficient route to graphene. *The Journal of Physical Chemistry C*, *115*, 11957–11961.